Advanced simulation of a PV module's color

Cite as: AIP Conference Proceedings **1999**, 020017 (2018); https://doi.org/10.1063/1.5049256
Published Online: 10 August 2018

Keith R. McIntosh, Mohamed Amara, Fabien Mandorlo, Malcolm D. Abbott, and Benjamin A. Sudbury

Advanced Simulation of a PV Module's Color

Keith R. McIntosh,[1, a)] Mohamed Amara,[2]
Fabien Mandorlo,[2] Malcolm D. Abbott[1] and Benjamin A. Sudbury[1]

[1]*PV Lighthouse, Coledale, NSW 2515, Australia*
[2] *Université de Lyon, Institut des Nanotechnologies de Lyon INL - UMR5270 CNRS*
INSA Lyon, F-69621, Villeurbanne, France

[a)] Corresponding author: krmcintosh@pvlighthouse.com.au

Abstract. We apply advanced ray tracing to predict the color of an encapsulated solar cell. Previous studies have predicted the color from the thickness and refractive index of the antireflection coating and encapsulants. Here, we demonstrate how other effects influence the color significantly, applying ray tracing to account for texture, for direct and diffuse insolation, for scattering, and for the observer angle. Despite the sophistication of the ray tracing, solutions for each simulation are attained within seconds. With an accurate and quick way to predict a module's color, researchers can avoid costly experimentation when (i) predicting how cell color will change after encapsulation, (ii) determining production tolerances to limit color variability within a cell or module and (iii) optimizing for a particular color for BIPV applications.

INTRODUCTION

Most crystalline-silicon solar cells appear dark blue, where the particular shade of blue depends on the cell's antireflection coating (ARC) and surface texture [1]–[6]. In some cases, variability in the ARC or texture leads to sufficient variability in the color that a module is deemed ugly and, irrespective of its electrical performance, is either rejected or sold at a lower price. Figure 1(a) illustrates how the shade of blue can vary between modules and sometimes between the cells of the same module.

Alternatively colored modules are often desired for BIPV applications [7]. This can be achieved by using a thick ARC [3], [4], dielectric nanoparticles [8], metal nanoparticles [9], tinted glass, pigmented coatings [10], and thin-film stacks [11], although there is always an accompanying reduction in efficiency. Figure 1(b) provides an example of a BIPV installation containing green c-Si modules.

Thus, whether to set production tolerances to limit color variability or to optimise the fabrication conditions to attain a particular color, it is useful for manufacturers to predict the color of an encapsulated cell. This paper concerns the application of ray tracing to predict color before and after encapsulation for any ARC thickness, texture, observation angle and incident illumination.

(a) (b)

FIGURE 1. (a) FraunhoferCSE testing facility in Albuquerque showing colour variation between modules and, in some cases, between solar cells within a module, and (b) BIPV rooftop with green modules. Photos courtesy of @FraunhoferCSE (www.cse.fraunhofer.org) and ColoredSolar (www.coloredsolar.com).

SiliconPV 2018, The 8th International Conference on Crystalline Silicon Photovoltaics
AIP Conf. Proc. 1999, 020017-1–020017-9; https://doi.org/10.1063/1.5049256
Published by AIP Publishing. 978-0-7354-1715-1/$30.00

GENERAL APPROACH TO SIMULATING COLOR

The general approach taken to simulate the color of a solar cell or module contains three steps [1], [2], [6], [7]: (1) to apply ray tracing to determine the reflected spectrum, (2) to multiply that spectrum by standard observer color matching functions to determine XYZ, and (3) to convert XYZ to RGB values to display the color on a monitor.

Step 1 usually involves simplifications to limit the complexity of the ray tracing. In particular, prior works have tended to consider hemispherical reflectance (not the reflectance for specific observation and acceptance angles), simple morphologies for surface texturing (considering just the major reflected paths and no scattering), and normally incident AM1.5g light (neglecting angles and spectra of diffuse and direct light). Studies on modules [2] have also omitted absorption in the encapsulants and ARC. Nevertheless, the general trends of color can be predicted, where a large range of colors can be obtained by varying the thickness or refractive index n of the ARC.

In this work, we apply SunSolve [12] to extend on prior investigations into module color, evaluating the relevance of diffuse and direct insolation, of observation and acceptance angles, and of scattering. The simulation inputs are selected to represent conventional modern solar cells and are listed in the appendix.

Although the focus of this paper relates to Step 1, we now make a few comments regarding our approach to Steps 2 and 3: (i) We do not present absolute XYZ but its normalized equivalent, *xyz*, where $x = X / (X + Y + Z)$, $y = Y / (X + Y + Z)$ and $z = Z / (X + Y + Z)$. This removes information about the color's luminosity, which we cannot deduce without specifying more information about the intensity of the incident light and the location of the observer. (ii) We present the results on an *xy* chromacity chart (e.g., Figure 2), where z can be determined as $z = 1 - x - y$. (iii) Results for RGB are determined for the sRGB color space, as developed by HP and Microsoft and applied by most modern monitors. (iv) To determine RGB, we linearly scale XYZ to give a luminosity of Y = 5%, and then convert XYZ to sRGB via standard equations [13][14] where the *xy* coordinates of the white point are {0.31271, 0.32903}. (v) When XYZ does not correspond exactly to a value in sRGB space, i.e., when the *xy* point lies outside the sRGB triangle, the calculated color cannot be represented by a standard computer monitor. To determine the 'nearest' RGB, we take the approach described by Walker [15] and illustrated by Figure 2, where we define the RGB to be the intercept between the dashed line that joins the *xy* point (circle) to the white point (square) and the nearest side of the sRGB triangle.

SIMULATING SOLAR CELLS

Several previous studies predicted cell color from direct or hemispherical reflectance and normally incident illumination [1][2][6]. Our results for this condition are presented in Figure 3(a) and the top line in Table 1 for three surface textures: planar, random pyramids and isotexture. The results indicate that all three surface textures appear blue, as is expected for solar cells coated with 75 nm of SiN_x. The color of the random-pyramid texture is found to be a purer blue; i.e., the *xy* point is further from the white point on the chromacity chart. We cannot precisely compare our *xy* points to those in [1][2] because the *xy* plots in those references do not specifically label the case of 75 nm, and

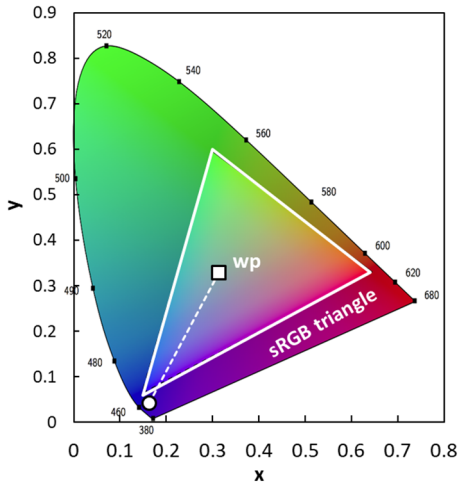

FIGURE 2. Example of when the calculated *xy* point (circle) lies outside the sRGB triangle. The white point (wp) is that for the D65 6504 K spectrum and has *xy* coordinates of {0.31271, 0.32903}. The calculated *xy* point is for a solar cell textured by random pyramids.

because of differences in the SiN_x refractive index; nevertheless, our *xy* points are similar to the 'bluest' *xy* points for planar [1][2] and textured [2] wafers, as expected for 75 nm of SiN_x.

Figure 3(b) and Table 1 also present the results when modifications are made to make the simulation better represent an observer viewing a solar cell in the field:

Firstly, the reflectance spectra that was used to determine the color was limited to a smaller observation (or detection) angle. Instead of the hemispherical reflectance, which incorporates reflected rays with a zenith angle within 0–90°, we restricted that range to 30–50°. This is the equivalent to placing the observer at 40° to the cells with an acceptance angle of ±10°. This is more accurate than solving for the hemispherical reflectance because it is not possible for an observer to detect light reflected at all angles from a solar cell. Since there is little or no azimuthal dependence in these cases, there was no reason to restrict the acceptance angle to a specific range of azimuth angles; by integrating over all azimuth angles, a superior signal-to-noise was attained for a given number of rays.

Secondly, we modified the incident illumination. Instead of the illumination emanating from a single source and being comprised of a normally incident AM1.5g (global) spectrum, the illumination emanated from dual sources comprised of the normally incident AM1.5d (direct) spectrum and an isotropic $AM1.5_{diffuse}$ spectrum (see appendix). Hence, the dual source contained the direct component at normal incidence and the diffuse component of the AM1.5 spectrum. This better represents sunlight because the spectrum of its diffuse light is much bluer than the spectrum of its direct light [16].

TABLE 1. Simulated *xy* points for an unencapsulated solar cell with one of three textures. Results provided for a detection angle range of either 0–90° (i.e. hemispherical) or 30–50° (e.g. observer at an angle) and for either a single or dual illumination source; the single source is the normally incident AM1.5g, and the dual source is both a normally incident AM1.5d spectrum and an isotropic $AM1.5_{diffuse}$ spectrum.

Detection angle	Illum. source	Planar		Random pyramids		Isotexture	
		x	*y*	*x*	*y*	*x*	*y*
0–90°	Single	0.171	0.140	0.164	0.083	0.181	0.141
0–90°	Dual	0.161	0.132	0.161	0.061	0.180	0.146
30–50°	Single	–	–	0.156	0.070	0.164	0.119
30–50°	Dual	0.170	0.104	0.158	0.059	0.163	0.124

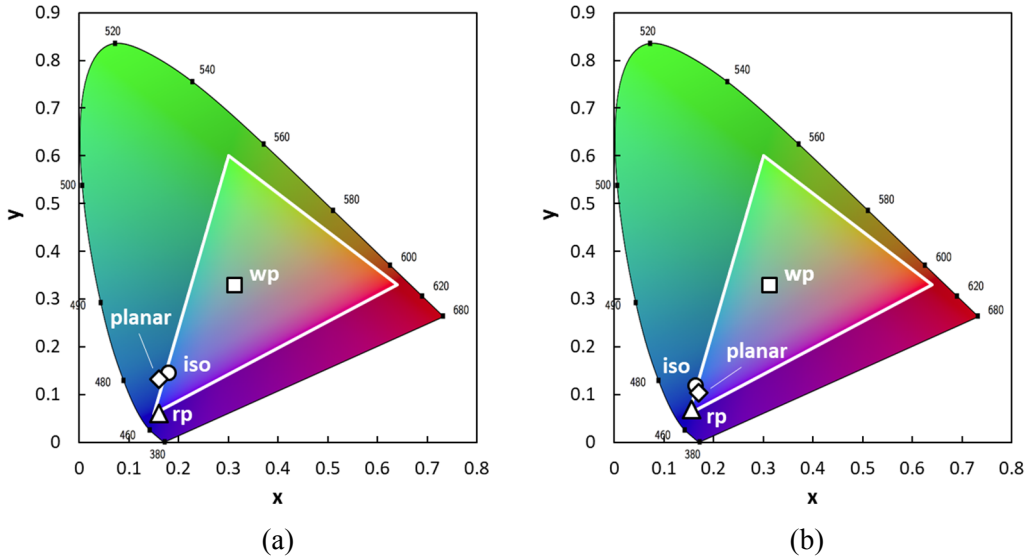

FIGURE 3. Simulated *xy* points for unencapsulated solar cells with (a) 0–90° detector angle and single illumination source and (b) 30–50° detector angle and dual illumination source. The front surface of the cells is either planar (diamonds), textured with random pyramids (triangles), or isotextured (circles); the white point is also shown (squares)..

TABLE 2. Simulated *xy* points for an encapsulated solar cell with one of three textures.

Detection angle	Illum. source	Random pyramids		Isotexture	
		x	*y*	*x*	*y*
0–90°	Single	0.323	0.320	0.302	0.298
0–90°	Dual	0.187	0.079	0.194	0.157
30–50°	Single	0.316	0.328	0.302	0.305
30–50°	Dual	0.281	0.278	0.238	0.224

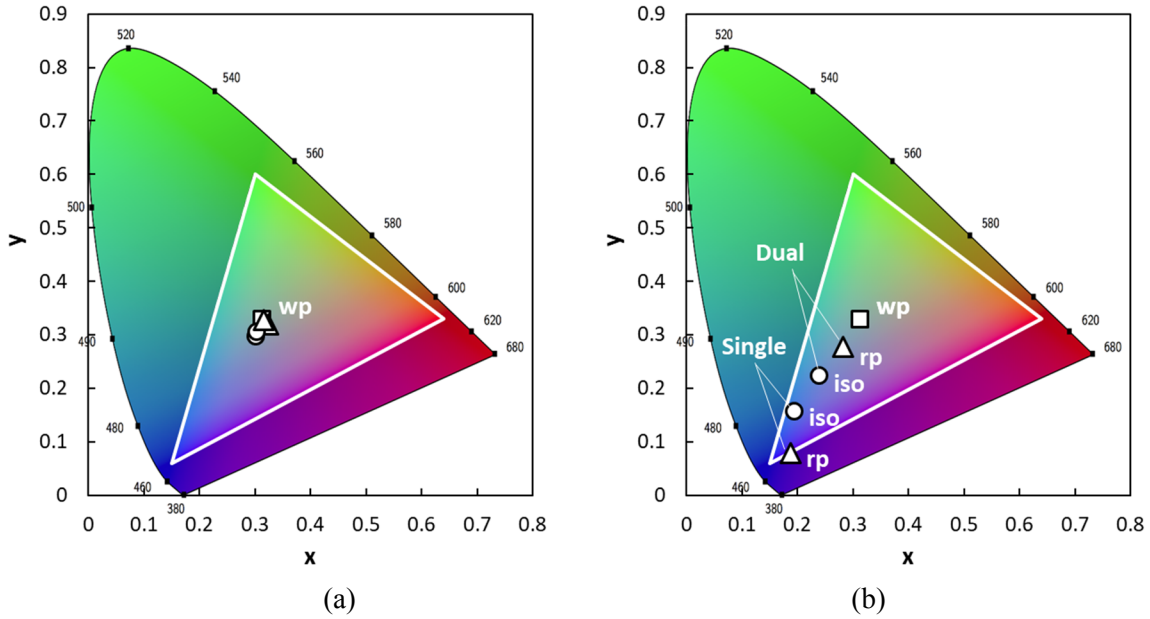

FIGURE 4. Simulated *xy* points for unencapsulated solar cells with a detector zenith angle of (a) 0–90° (hemispherical) and (b) 30–50°. Both graphs contain points for single and dual illumination sources.

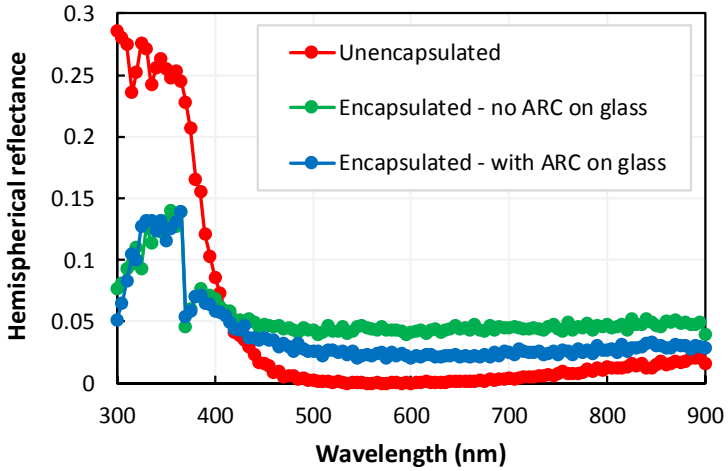

FIGURE 5. Simulated reflectance for an unencapsulated solar cell textured with random pyramids coated with 75 nm of SiN_x before and after encapsulation with and without an ARC on the glass.

Figure 3 and Table 1 indicate that when these two complications are included, there is a small change to the predicted color: the *xy* points become 'bluer', shifting further from the white point and, in the case of planar and isotextured cells, containing slightly less green.

Whether the change in *xy* constitutes a significant difference depends on the accuracy of interest, although we emphasize that other differences between experiment and simulation (e.g., in the properties of the SiN_x or texture) might lead to a greater error in the *xy* point than arises from this improved representation of the spectrum and observation angle. The next section shows that the improved representation is much more significant for encapsulated solar cells.

SIMULATING MODULES

For encapsulated solar cells, the two aforementioned modifications make a big difference to the predicted color. This can be seen from the results presented in Figure 4 and Table 2 (planar case omitted). Figure 4(a) presents the results for a detector angle of 0–90° (hemispherical) and 4(b) presents the results for the restricted detector angle of 30–50°.

As evident in Figure 4(a), all simulations that account for the hemispherical reflectance yield a color very close to the white point. Depending on the observing conditions and ambient lighting, they will appear either white or gray. The reason the predicted *xy* point is near the white point is that, as shown in Figure 5, the glass reflects approximately uniformly at all relevant wavelengths. Even with a glass ARC, the dependence of reflectance on wavelength is small compared to the unencapsulated case. Since the majority of the reflected light is that reflected by the glass, the perceived color is approximately the same as the sun's color (nearly white). When the light that is specularly reflected by the glass is neglected by restricting the observer angle to 40±10°, the *xy* points shift away from the white point and towards the blue region of the *xy* chart, as shown in Figure 4(b). Removing this glass reflection is clearly required before predicting module color, as was effectively performed in [2] but for normally incident light and a single ray path.

The *xy* points also depend significantly on whether the incident illumination was from the dual or single illumination sources. With the dual source, the color is less blue. In the single-source case, none of the light reflected by the glass reaches the detector; instead, the detector receives only light reflected from the cell, which is predominantly blue. For the dual-source case, some of the isotropic light is reflected from the glass and towards the detector. Although this diffuse light is bluer than the direct light, the glass reflectance is broadband and more long-wavelength photons contribute to the signal. Hence, the simulated color is less blue when the dual spectrum is introduced, particularly for cells with random-pyramid texturing.

It is clear from these results that an accurate simulation of module color requires setting an appropriate observer and acceptance angles as well as accounting for the direct and isotropic nature of illumination.

We now extend the module simulations to examine how its color is affected by (i) the thickness of the SiN_x anti-reflective coating between the solar cell and the EVA, (ii) the observation angle, and (iii) scattering from the cell surface. Note that the results are specific to the inputs stated in the appendix but SunSolve can be used to rapidly repeat these simulations with alternative inputs.

SIN_X THICKNESS

Figure 6 plots how cell color and generation current density J_{gen} depend on SiN_x thickness before and after encapsulation. This example was simulated for the baseline isotextured solar cell using the aforementioned dual-illumination source and detector angles. The figure shows that small changes to the SiN_x thickness lead to significantly different shades of blue for the solar cell, but that these differences are largely suppressed after encapsulation (consistent with [2]). It also shows that significant differences in color do not necessarily correlate to significant differences in J_{gen}. For example, unencapsulated cells with an SiN_x thickness of 65, 75 and 85 nm are predicted to appear as deep purple, dark blue and navy blue solar cells, while their J_{gen} differs by no more than 1%. Note that these colors were computed for the AM1.5 spectrum and would appear slightly differently under the fluorescent lighting of a laboratory or under a different air mass; the color under alternative spectra could also be simulated.

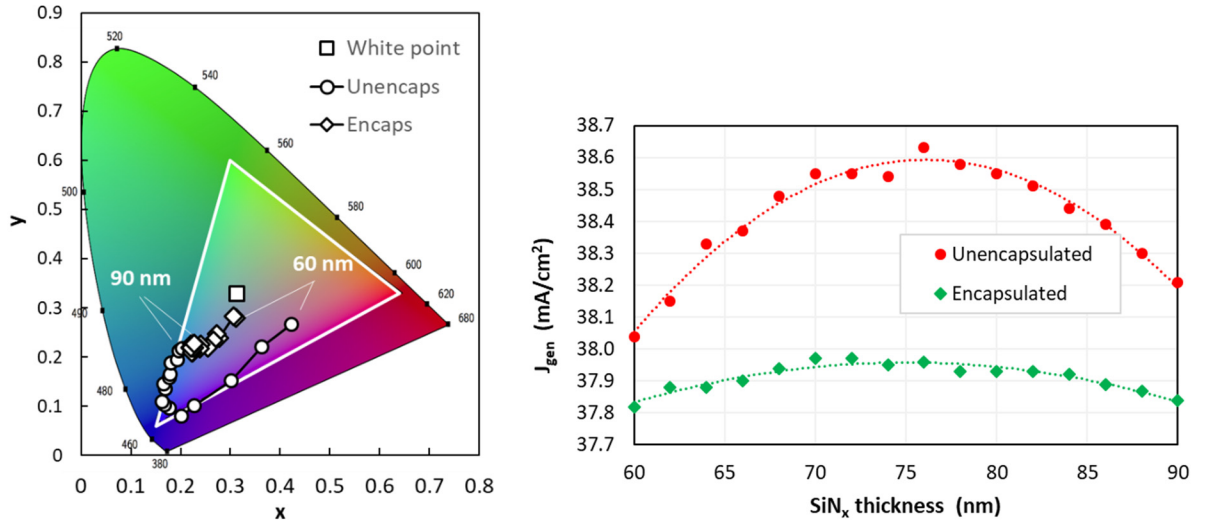

(c)

60 nm	62 nm	64 nm	66 nm	68 nm	70 nm	72 nm	74 nm	76 nm	78 nm	80 nm	82 nm	84 nm	86 nm	88 nm	90 nm
(96,49,60)	(97,45,79)	(96,42,99)	(90,40,120)	(79,42,134)	(62,48,139)	(48,52,140)	(36,56,137)	(21,60,131)	(8,61,129)	(9,63,122)	(12,63,119)	(10,65,111)	(21,65,109)	(22,65,105)	(23,66,102)

(d)

60 nm	62 nm	64 nm	66 nm	68 nm	70 nm	72 nm	74 nm	76 nm	78 nm	80 nm	82 nm	84 nm	86 nm	88 nm	90 nm
(69,62,62)	(69,61,63)	(67,62,64)	(67,62,64)	(66,62,65)	(66,62,69)	(66,62,68)	(66,62,69)	(63,63,70)	(64,62,70)	(66,61,72)	(63,62,73)	(63,62,76)	(61,63,74)	(61,63,74)	(60,63,74)

FIGURE 6. Color and J_{gen} vs SiN_x thickness for an isotextured solar cell before and after encapsulation showing (a) *xy* for all SiN_x thicknesses, (b) J_{gen} vs SiN_x thickness, (c) and (d) predicted color and (R, G, B) for unencapsulated and encapsulated cells, respectively, assuming a luminosity of Y = 5%. The appearance of the colors in (c) and (d) will depend on the calibration of the reader's monitor or printer.

OBSERVATION ANGLE

Figure 7 shows how the color of a module depends on the observation angle. As above, this example was simulated for the baseline encapsulated isotextured solar cell using the aforementioned dual-illumination source but where the zenith angle of the detector (i.e., the observer) is swept from 0 to 85° relative to the plane of the module. The acceptance angle remained at ±10° for all simulations, and it was again assumed that there was no azimuthal dependence, which introduces no loss in accuracy for isotextured wafers.

The figure shows that when the observer is near normal, the simulated *xy* point is near the white point. This is because the direct sunlight is reflected from the glass into the observer's eyes; due to the broadband nature of the glass reflectance, the observer is effectively seeing the sun's reflection.

Figure 7 also shows that when the observer's angle exceeds 10°, the observer no longer detects the specular reflectance from the glass and the cells appear blue again. Furthermore, the color becomes increasingly less blue (and slightly redder) as the observer's angle increases beyond 10°. This is because at this angle, a smaller fraction of light that is reflected multiple times from the spherical caps reaches the detector.

Note that the RGB values of Fig. 7b were calculated for a luminosity of Y = 5% whereas, in practice, the luminosity—and hence the values for R, G and B—would be much brighter for the near-normal detector angles. The purpose of Fig 7b is to illustrate that there is a dramatic change in color as the detector angle changes, rather than to provide accurate values of RGB.

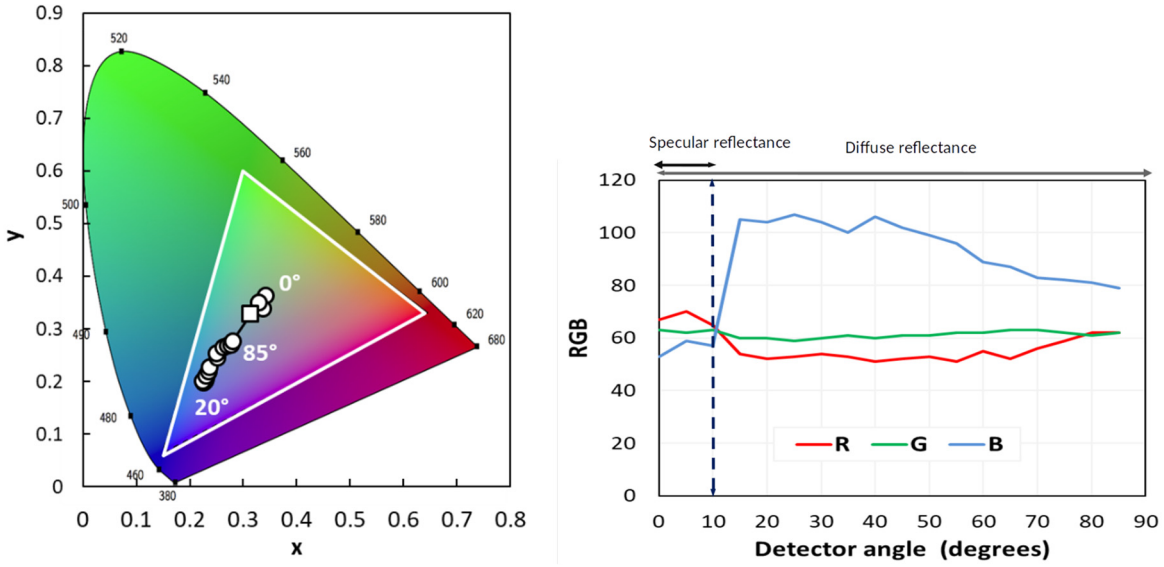

(a) (b)

FIGURE 7. Simulated generation current J_{gen} vs SiN_x thickness for an isotextured solar cell before and after encapsulation under the dual illumination source with a detector zenith angle within 30–50°. For figure b both specular and diffused light are normalized with Y=5%, so we cannot compare the left to the right side of the figure.

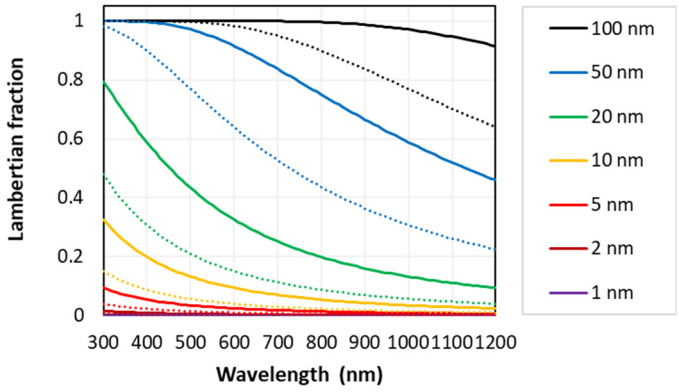

FIGURE 8. Scattering fraction as a function of wavelength and σ_{RMS} for an incident medium of $n = 1.5$ where the incident angle is either 0° (solid) or 50° (dotted) as determined from the scalar-scattering model [17], [18].

SCATTERING

Scattering from the surface of the solar cell arises due to its large-scale texture (pyramids, spherical caps) but also arise due to small-scale structure. To simulate this, we apply the scalar scattering model from [17], which leads to a greater fraction of shorter-wavelength rays scattering than longer-wavelength rays. Figure 8 plots how this scattering fraction depends on the wavelength and σ_{RMS} for normally incident light, where σ_{RMS} is the root-mean-square of the surface roughness. The scattering fraction also depends on the incident angle [17][18].

Figure 9 plots the resulting (a) *xy* and (b) RGB for the encapsulated random-pyramid solar cell as σ_{RMS} increases from 0 to 200 nm. Again, we see significant changes in the color of the module where the color becomes less green and more red as σ_{RMS} exceeds 10 nm and the fraction of long-wavelength light scattered towards the detector increases.

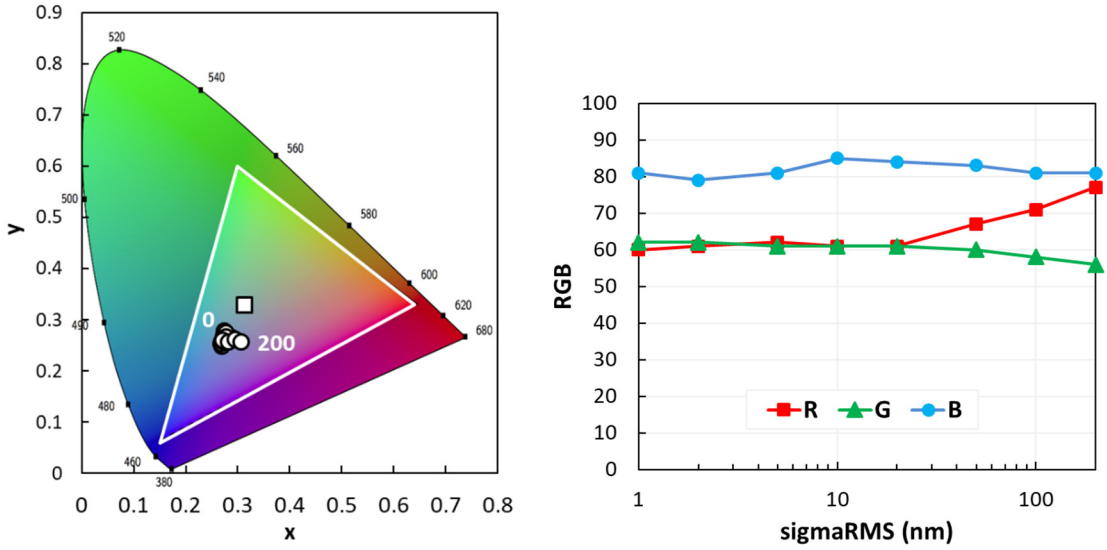

(a) (b)

FIGURE 9. Simulated generation current J_{gen} vs SiN_x thickness for an isotextured solar cell before and after encapsulation under the dual illumination source with a detector zenith angle within 30–50°.

CONCLUSIONS

This paper examined how the prediction of cell and module color depends on SiN_x thickness, texture morphology, observer angle, direct and diffuse spectra, and scattering from small-scale structure in the surface. All of these variables can have a significant impact for modules and hence an accurate prediction of a module's color requires sophisticated simulation.

APPENDIX

The ray tracing in this study was performed with SunSolve [12], [19]. Unless otherwise specified, the inputs for the ray tracing were as follows: The thickness of the glass, EVA, SiN_x and Si was 2 mm, 450 µm, 75 nm and 180 µm (excluding the height of the texture); $n(\lambda)$ and $k(\lambda)$ of glass, EVA, SiN_x and c-Si were taken from [20]–[23], the random pyramids were 5 µm high with a base angle of 53° where the randomization was treated as described in [24]; isotexture was represented as spherical caps [25] that were 2 µm high with a characteristic angle of 60°, which approximates the texture from commercial cells [26], where the rays were traced as described in [27]; the rear surface of the cell was planar with a reflectance of 70% and a Lambertian fraction of 80% (representing fired Al screen-print paste); the incident polarization was assumed randomized and changes in polarization were accounted for at every interaction between a ray and an interface; the wavelength range was 300 to 1200 nm in 2 nm intervals; the single-illumination source consisted of a normally incident AM1.5g spectrum; the dual-illumination source consisted of a normally incident AM1.5d spectrum and an isotropic $AM1.5_{diffuse}$ spectrum where the spectral intensity of $AM1.5_{diffuse}$ at each λ was calculated as $2 \times [AM1.5g(\lambda) - AM1.5d(\lambda)]$ where the factor of 2 ensures that the total spectral intensity incident for the dual-illumination source is identical to the single-illumination source; the number of rays traced was 500,000; the detector signal was limited to include only those rays that reflect from the cell or module within a zenith angle of $\theta = 30–50°$ and with no limit on azimuth angle; and the effects of the metal grid and backsheet were neglected. When solved on 200 parallel cores, solutions for these inputs were completed in a few seconds.

REFERENCES

[1] M. Amara, F. Mandorlo, R. Couderc, F. Gérenton, and M. Lemiti, "Temperature and color management of Silicon solar cells for building integrated photovoltaic," *EPJ Photovoltaics*, no. In press, pp. 1–11, 2017.

[2] I. Tobias, A. El Moussaoni, and A. Luque, "Colored solar cells with minimal current mismatch," *Electron*

Devices, IEEE, vol. 46, no. 9, pp. 1858–1865, 1999.
[3] J. H. Selj, T. T. Mongstad, R. Søndenå, and E. S. Marstein, "Reduction of optical losses in colored solar cells with multilayer antireflection coatings," *Sol. Energy Mater. Sol. Cells*, vol. 95, no. 9, pp. 2576–2582, 2011.
[4] M. Li, L. Zeng, Y. Chen, L. Zhuang, X. Wang, and H. Shen, "Realization of Colored Multicrystalline Silicon Solar Cells with SiO 2 /SiN x :H Double Layer Antireflection Coatings," *Int. J. Photoenergy*, vol. 2013, pp. 1–8, 2013.
[5] N. Ishikawa *et al.*, "PV modules, using color solar cells, designed for building," *Proc. 1994 IEEE 1st World Conf. Photovolt. Energy Convers. - WCPEC (A Jt. Conf. PVSC, PVSEC PSEC)*, vol. 1, pp. 977–980 vol.1, 1994.
[6] Y. Chen, Y. Yang, Z. Feng, P. P. Altermatt, and H. Shen, "Color Modulation of c-Si Solar Cells without significant Current-loss by Means of a Double-layer Anti-reflective Coating," *27th EUPVSEC*, 2012.
[7] Q. Bao, T. Honda, S. El Ferik, M. M. Shaukat, and M. C. Yang, "Understanding the role of visual appeal in consumer preference for residential solar panels," *Renew. Energy*, vol. 113, pp. 1569–1579, 2017.
[8] G. Peharz *et al.*, "Application of plasmonic coloring for making building integrated PV modules comprising of green solar cells," *Renew. Energy*, vol. 109, pp. 542–550, 2017.
[9] D. L. King, "Photovoltaic Module and Array Performance Characterization Methods for All System Operating Conditions," *Rev. Lit. Arts Am.*, pp. 1–22, 1997.
[10] S. K, J. Noopur, and B. Shivani, "Effect of color filter on the performance of solar photovoltaic module," in *2013 International Conference on Power, Energy and Control (ICPEC) EFFECT*, 2013, pp. 35–38.
[11] L. Wen, Q. Chen, F. Sun, S. Song, L. Jin, and Y. Yu, "Theoretical design of multi-colored semi-transparent organic solar cells with both efficient color filtering and light harvesting.," *Sci. Rep.*, vol. 4, p. 7036, Nov. 2014.
[12] "SunSolve." [Online]. Available: www.pvlighthouse.com.au/sunsolve. [Accessed: 18-Mar-2018].
[13] R. Juckett, "RGB Color Space Conversion." [Online]. Available: http://www.ryanjuckett.com/programming/rgb-color-space-conversion. [Accessed: 19-Mar-2018].
[14] "sRGB." [Online]. Available: https://en.wikipedia.org/wiki/SRGB. [Accessed: 19-Mar-2018].
[15] J. Walker, "Colour Rendering of Spectra." [Online]. Available: https://www.fourmilab.ch/documents/specrend. [Accessed: 19-Mar-2018].
[16] C. A. Gueymard, "Parameterized transmittance model for direct beam and circumsolar spectral irradiance," *Sol. Energy*, vol. 71, no. 5, pp. 325–346, 2001.
[17] C. K. Carniglia, "Scalar Scattering Theory for Multilayer Optical Coatings," *Opt. Eng.*, vol. 18, no. 2, p. 182104, Apr. 1979.
[18] D. Dominé, F.-J. Haug, C. Battaglia, and C. Ballif, "Modeling of light scattering from micro-and nanotextured surfaces," *J. Appl. Phys.*, vol. 107, no. 4, p. 44504, 2010.
[19] M. D. Abbott, K. R. McIntosh and B. A. Sudbury, "Optical loss analysis of pv modules," *EU PVSEC Proc.*, 2016.
[20] K. R. McIntosh *et al.*, "Increase in external quantum efficiency of encapsulated silicon solar cells from a luminescent down-shifting layer," *Prog. Photovoltaics Res. Appl.*, vol. 17, no. 3, pp. 191–197, May 2009.
[21] K. R. Mcintosh, J. N. Cotsell, J. S. Cumpston, A. W. Norris, N. E. Powell, and B. M. Ketola, "An optical comparison of silicone and EVA encapsulants for conventional silicon PV modules: a ray-tracing study," in *34th IEEE Photovoltaic Specialists Conference*, 2009, pp. 544–549.
[22] M. R. Vogt, "Development of Physical Models for the Simulation of Optical Properties of Solar Cell Modules," Leibniz University, 2015.
[23] M. A. Green, "Self-consistent optical parameters of intrinsic silicon at 300 K including temperature coefficients," *Sol. Energy Mater. Sol. Cells*, vol. 92, no. 11, pp. 1305–1310, 2008.
[24] S. C. Baker-Finch and K. R. McIntosh, "Reflection of normally incident light from silicon solar cells with pyramidal texture," *Prog. Photovoltaics Res. Appl.*, vol. 19, no. 4, pp. 406–416, 2011.
[25] S. C. Baker-finch, K. R. Mcintosh, M. L. Terry, and a H. Reflectance, "Isotextured Silicon Solar Cell Analysis and Modeling 1 : Optics," *IEEE J. Photovoltaics*, vol. 2, no. 4, pp. 457–464, 2012.
[26] S. Wasmer, J. Greulich, H. Höffler, J. Haunschild, M. Demant, and S. Rein, "Investigating the impact of parameter and process variations on multicrystalline silicon PERC cell efficiency," in *Proc. 31st Eur. Photovoltaic Sol. Energy Conf. Exhib.*, 2015.
[27] K. R. McIntosh, M. D. Abbott, and B. A. Sudbury, "Ray tracing isotextured solar cells," *Energy Procedia*, vol. 92, pp. 122–129, 2016.